LETTER

Plasmonic nanopatch array with integrated metal–organic framework for enhanced infrared absorption gas sensing

To cite this article: Xinyuan Chong *et al* 2017 *Nanotechnology* **28** 26LT01

View the article online for updates and enhancements.

Related content

- Plasmon resonance tuning in metal nanostars for surface enhanced Raman scattering
  Manohar Chirumamilla, Anisha Gopalakrishnan, Andrea Toma et al.
- Diffusion and photoswitching in nanoporous thin films of metal-organic frameworks
  Lars Heinke
- Roadmap on biosensing and photonics with advanced nano-optical methods
  Enzo Di Fabrizio, Sebastian Schlücker, Jérôme Wenger et al.

Recent citations

- Optimally designed gold nanorattles with strong built-in hotspots and weak polarization dependence
  Xuemin Zhang *et al*

This content was downloaded from IP address 128.193.154.71 on 22/01/2018 at 19:21

IOP Publishing
Letters
Nanotechnology
Nanotechnology **28** (2017) 26LT01 (7pp)
https://doi.org/10.1088/1361-6528/aa7433

Letter

Plasmonic nanopatch array with integrated metal–organic framework for enhanced infrared absorption gas sensing

Xinyuan Chong[1], Ki-joong Kim[2,3,4], Yujing Zhang[2], Erwen Li[1], Paul R Ohodnicki[3,5], Chih-Hung Chang[2] and Alan X Wang[1]

[1] School of Electrical Engineering and Computer Science, Oregon State University, Corvallis, OR 97331, United States of America
[2] School of Chemical, Biological and Environmental Engineering, Oregon State University, Corvallis, OR 97331, United States of America
[3] National Energy Technology Laboratory (NETL), US Department of Energy, 626 Cochrans Mill Road, Pittsburgh, PA 15236, United States of America
[4] AECOM, 626 Cochrans Mill Road, Pittsburgh, PA 15236, United States of America
[5] Materials Science and Engineering, Department, Carnegie Mellon University, Pittsburgh, PA 15213, United States of America

E-mail: wang@eecs.oregonstate.edu

Received 14 March 2017, revised 8 May 2017
Accepted for publication 19 May 2017
Published 6 June 2017

Abstract

In this letter, we present a nanophotonic device consisting of plasmonic nanopatch array (NPA) with integrated metal–organic framework (MOF) for enhanced infrared absorption gas sensing. By designing a gold NPA on a sapphire substrate, we are able to achieve enhanced optical field that spatially overlaps with the MOF layer, which can adsorb carbon dioxide (CO_2) with high capacity. Experimental results show that this hybrid plasmonic–MOF device can effectively increase the infrared absorption path of on-chip gas sensors by more than 1100-fold. The demonstration of infrared absorption spectroscopy of CO_2 using the hybrid plasmonic–MOF device proves a promising strategy for future on-chip gas sensing with ultra-compact size.

Keywords: plasmonics, gas sensing, metal–organic framework, infrared absorption

(Some figures may appear in colour only in the online journal)

Introduction

Metal–organic frameworks (MOFs), a new class of nanoporous materials, have attracted intensive research interests due to their large surface area and wide structure tunability. MOFs are extended crystalline structures consisting of metal ions connected by organic ligands, which can essentially possess an infinite number of possible combinations with different physical and chemical properties. Therefore, MOFs have been widely applied in chemical separation [1], gas storage [2–5], drug delivery [6], sensing [7–10], and catalysis [11–14] applications. In recent years, hybrid plasmonic–MOF nanostructures have been reported to take the advantages of the strong gas adsorption capabilities of MOF materials and the optical field enhancement of plasmonics effect. These hybrid nanostructures have been applied in different applications, such as catalysis [15–18], imaging [19], surface-enhanced Raman scattering [20–27] and surface-enhanced infrared absorption [9]. However, most of these reported hybrid plasmonic–MOF nanostructures are based on chemically synthesized metallic or semiconductor nanoparticles, which have several drawbacks. First, the optical field enhancement of plasmonic nanoparticles (NPs) comes from the intrinsic plasmonic resonance of free electrons, which has

 © 2017 IOP Publishing Ltd Printed in the UK

strong optical scattering and relatively low quality-factors (Q-factors) of only about 4–5. Considering a large amount of randomly distributed plasmonic NPs, the optical transmission through the thin film is relatively low. Second, the enhanced optical field from intrinsic plasmonics effect of NPs are highly localized, mostly confined at the surface or between the NPs. This means that the hot spot volume is very limited. Only the analyte molecules within the hot spot can interact with the highly localized optical field. For example, in our previous work [9], the volume ratio of the hot spots in the hybrid indium tin oxide NPs with Cu–BTC (BTC = benzene-1, 3, 5-tricarboxylate) MOF to enhance gas absorption is only 0.12% based on our numerical calculation. Therefore, the overall plasmonic field enhancement is only about 2.6 times from our numerical calculation. Last, the intrinsic plasmonic resonance of chemically synthesized NPs is affected by free electron concentration, composition, size, geometry, and even the coupling between the NPs, which is difficult to control. Many experimentally results actually show much broader plasmonic resonances than simulation due to the inherent limitations and variation of fabrication process.

In this paper, we present a nanophotonic device consisting of a periodic plasmonic nanopatch array (NPA) [28] with integrated MOF layer to resolve the engineering challenges. Compared with randomly distributed plasmonic NPs relying on the intrinsic plasmonics effect [9] or triangular dipole nano-antennas with MOF [29], our design offers much higher Q-factors with higher optical transmission efficiency due to the constructive interaction of the surface plasmon polaritons at the interface between a gold (Au)-NPA and MOF thin film [30]. The optical field at the surface of the plasmonic NPA extends to the entire MOF layer, which can effectively increase the strength of light–matter interaction. In other words, more analyte molecules can be adsorbed and concentrated inside the MOF film and interact with the plasmonic field, which is crucial for enhanced infrared absorption. Moreover, the plasmonic resonance can be fine-tuned by the periodicity of the NPA, which can be precisely controlled by top-down lithography process. The large and precision tunability of plasmonic resonances offers the possibility to enhance the vibrational spectra sensing of various analytes and even for multiplexed sensing with high throughput.

The device consists of a Au-NPA on a sapphire ($n_{\text{sapphire}} = 1.721$) substrate, which is covered by a thin layer of MOF ($n_{\text{MOF}} = 1.326$), zeolitic imidazolate frameworks (ZIFs) or ZIF-8, as shown in figure 1. Light is launched from the MOF side, and the transmitted light is collected from the substrate. When the light is coupled into the device normal to the surface, surface plasmon resonances are excited at the Au/MOF interface and coupled with the Fabry–Pérot modes in the MOF layer as well. Since the Au-NPA is symmetric, the device is polarization independent. Based on the design, the parameters that can be modified are the periodicity (P) of the Au-NPA, gap width (G) between Au-NPs, the thickness (H) of the MOF layer and the Au thickness (T). In order to achieve high optical field enhancement within the MOF layer, optimization is performed by the DiffractMOD of Rsoft

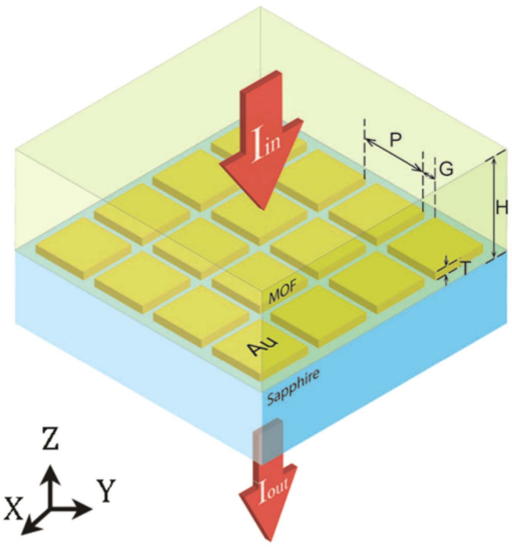

Figure 1. Schematic of the MOF integrated plasmonic nanopatch array. For geometrical parameters, P is the gold nanopatch period, G is the nano-slit width, H is the MOF thickness and T is the gold thickness. I_{in} and I_{out} stand for the intensity of the incident and transmitted light.

photonic component design suite, which is based on rigorous coupled-wave analysis [31]. Among these parameters, the MOF thickness (H) is the most important one. The optical effect of the parameters is well-studied in the literature for plasmonic nano-antennas [32]. The periodicity (P) of the Au-NPA determines the peak wavelength; the gap (G) affects the transmission intensity and also the spectrum width; the Au thickness (T) also has an influence on the transmission intensity. In this paper, we focused on the detailed study of the MOF thickness (H) as it not only affects the optical field enhancement, but also determines the infrared absorption path.

A scanning of the MOF thickness (H) is performed by fixing other parameters. The transmission intensity results are shown in figure 2(a). The major peak (indicated by the white arrow) shows a red-shift when the MOF thickness (H) increases from 0.4 to 3.0 μm. For real applications, the transmission intensity should be high enough to obtain good signal-to-noise ratio. Thus, the three peaks in the simulated transmission spectrum for $H = 2.7$ μm shown in figure 2(b) with over 50% transmission efficiency provide excellent measurement condition. In order to verify whether the thickness (H) is appropriate, three different values are selected from the three regions represented by the white dash lines. The electric field distributions of the three values of thickness at peak at 2.7 μm after modifying the period are shown in figures 2(c)–(e). For $H = 0.5$ μm, it has the highest field intensity, but most of the enhanced field is in air instead of in the MOF layer, which is not preferred by gas sensing. For $H = 1.5$ and 2.7 μm, most of the field is confined in the MOF layer. If we only consider the plasmonic field, then $H = 1.5$ μm is better than $H = 2.7$ μm. However, we need to consider the amount of adsorbed gas by MOF in our design. In other words, a thinner MOF layer means less gas molecules

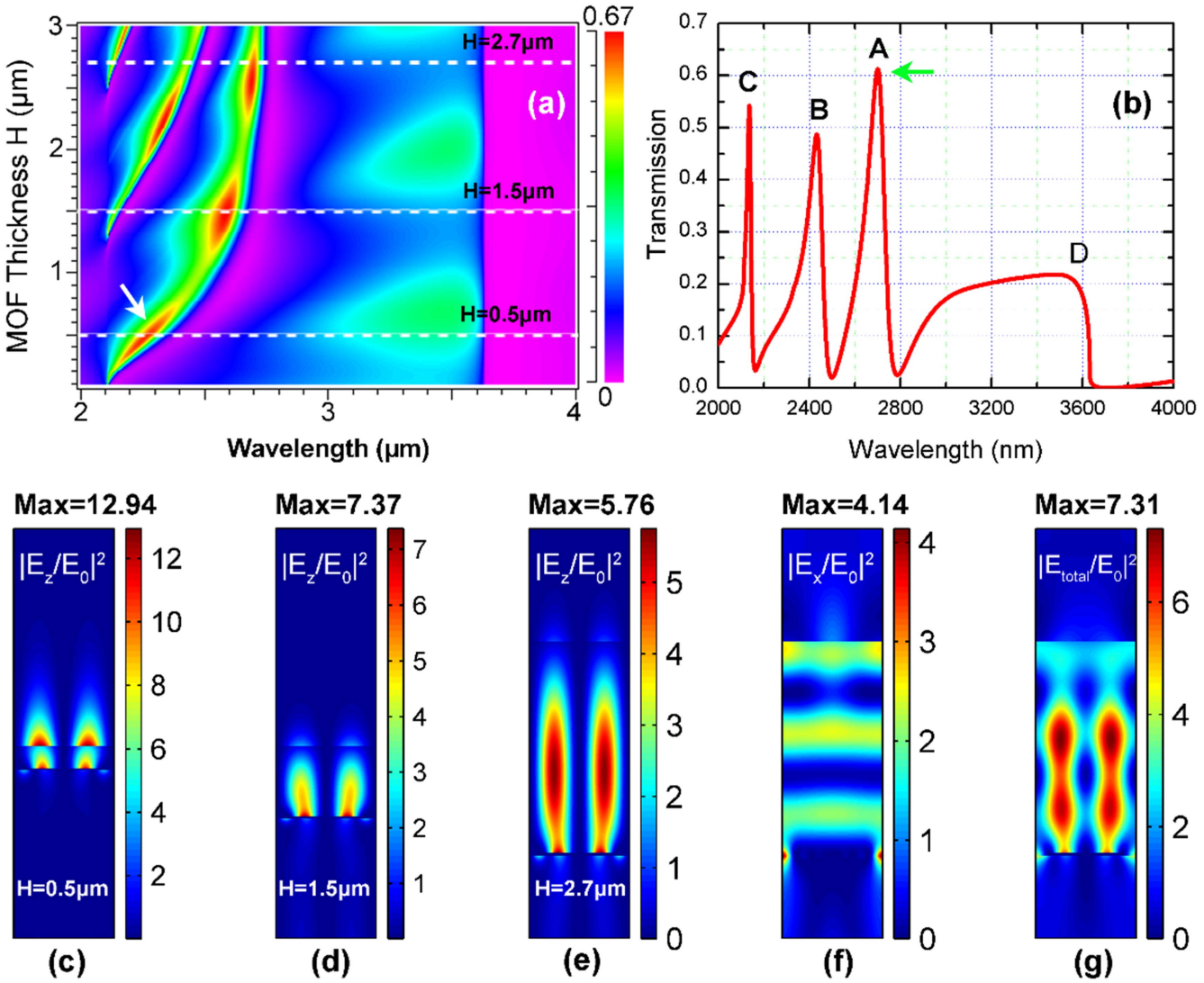

Figure 2. (a) Effect of the MOF thickness H in transmission intensity, with fixed P, T and G. The color bar represents the transmission intensity. (b) Simulated transmission spectrum for $H = 2.7\ \mu$m. Electric distribution of z direction for (c) $H = 0.5\ \mu$m, (d) $H = 1.5\ \mu$m and (e) $H = 2.7\ \mu$m. (f) The electric field distribution of (f) x direction, and (g) the summation of all directions for $H = 2.7\ \mu$m.

are adsorbed. Therefore, the relatively thicker MOF is more desirable to allow more gas molecules to interact with the optical field. Finally, after comprehensive consideration of the plasmonic effect, MOF's adsorbing property, transmission intensity and also growth time for the MOF layer, the parameters are determined to be $P = 2.11\ \mu$m, $G = 250$ nm, $H = 2.7\ \mu$m, and $T = 40$ nm. The simulated transmission spectrum is shown in figure 2(e), which has three resonant peaks in the shorter wavelength range and one sharp edge at the longer wavelength. Peak A is the desired coupled mode with ~60% transmission efficiency with a relatively higher Q-factor of 27.44. The electric field distributions at peak A are shown in figure 2(e) (E_z only, corresponding to the plasmonic resonance of the Au-NPA), figure 2(f) (E_x only, corresponding to the F–P resonance in the MOF thin film) and figure 2(g) (total hybridized electric field). The maximum intensity enhancement is 7.31. Essentially, the coupled mode extends the highly localized plasmonic field to the entire MOF layer, resulting in an increase of the interaction between gas molecules inside the MOF and the optical field. Peak B and C are the higher modes of peak A, and the sharp edge D represents the Rayleigh anomaly at the substrate side [33].

Experiments and results

The device is fabricated by focused ion beam etching followed by monolithic growth of a MOF thin film. The selected MOF is the zeolitic imidazolate framework-8 (ZIF-8s), which has been extensively investigated due to its excellent thermal stability and selectivity toward CO_2 [34]. Besides, due to the hydrophobic surface property, water molecules can only be adsorbed at the outer surface, while CO_2 can diffuse into the inner pores. Besides, the hydrophobic surface makes ZIF-8 even more attractive for chemical sensing in environments where water vapors are pervasive [34]. The growth process is described here briefly. Before growing the ZIF-8 film, the substrate with Au-NPA is cleaned in piranha solution

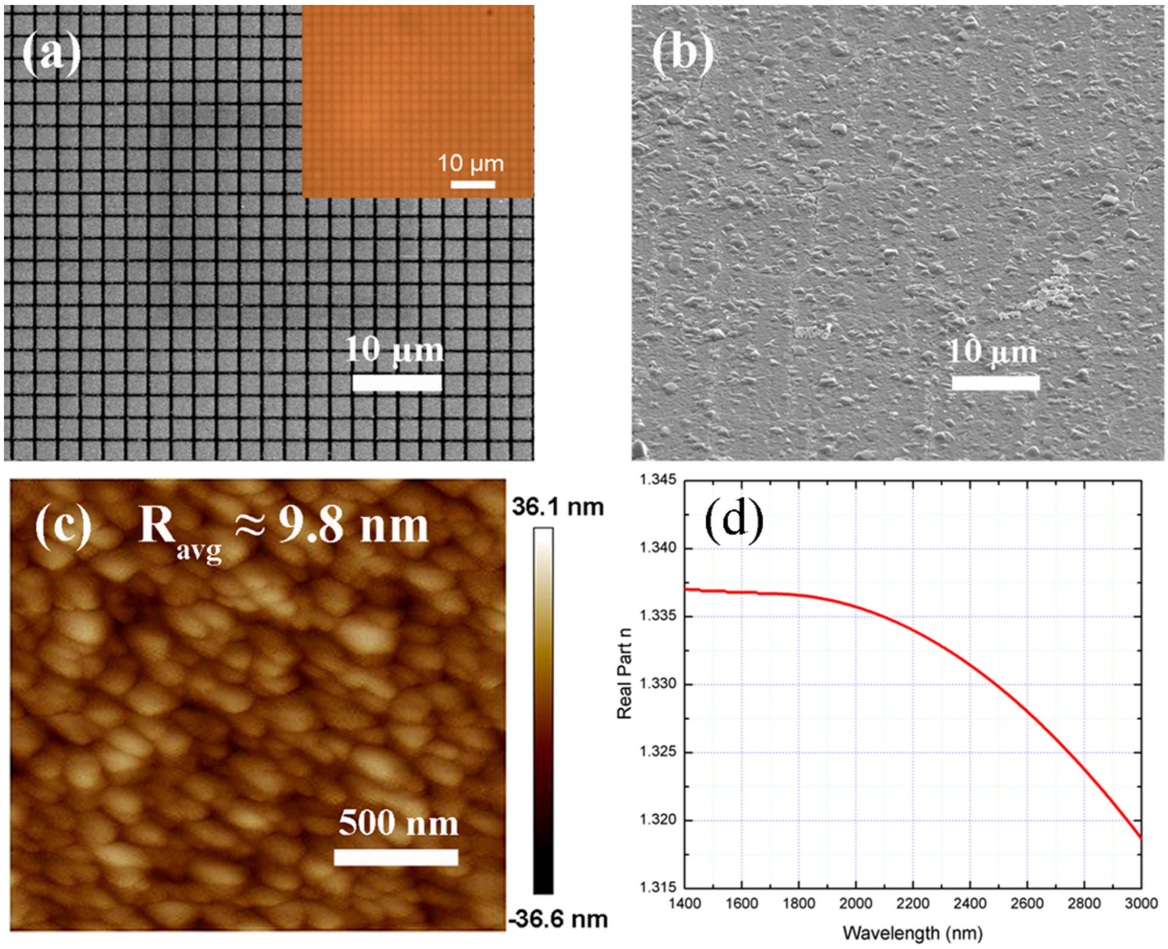

Figure 3. (a) SEM image of fabricated Au-NPA. The inset is the optical image of the Au-NPA. (b) The SEM image of Au-NPA after growing MOF. (c) AFM image of the ZIF-8 thin film. (d) The refractive index of the MOF thin film.

(H_2SO_4/H_2O_2, 70/30 v/v%) at 70 °C for 30 min. Then it is washed thoroughly by deionized water and dried under nitrogen flow. To grow ZIF-8 thin film, the cleaned Au-NPA sample is immersed in a freshly mixed methanolic solution of 2-methylimidazole and $Zn(NO_3)_2$ for 30 min at room temperature, followed by washing using methanol and drying under nitrogen flow. To obtain 2.7 μm MOF layer, this process is repeated for 32 cycles. The scanning electron microscope images of the fabricated Au-NPA before and after growing MOF are shown in figures 3(a) and (b), respectively. As we can see, the MOF layer fully covers the Au-NPA and the MOF forms a relative smooth thin film with surface roughness about 10 nm, which is measured by atomic force microscopy (AFM) as shown in figure 3(c). The refractive index of the MOF thin film coated on a silicon wafer was measured by elliposometry as shown in figure 3(d).

In order to quantitatively determine the enhancement provided by the hybrid plasmonic–MOF device, a CO_2 sensing measurement was performed by a Fourier transform infrared spectrometer system shown in figure 4(a). The gas cell used in the system is home built with 4 mm light path length. One side of the gas cell is sealed by a sapphire window and the other side is sealed by the device. Different CO_2 concentrations are obtained by mixing with nitrogen (N_2) using two mass flow controllers. Figure 4(b) shows the transmission spectra of different CO_2 concentration. As a reference, the hybrid plasmonic–MOF device is replaced by bare sapphire window. As a comparison, the transmission spectra of the reference without any device are shown in figure 4(c). The spectra in the manuscript have already been excluded from the effect of the plasmonic structure itself. Before taking the spectra of with CO_2, we measured the spectra of the device purged by Ar as reference. Since Ar molecules have no IR absorption around 2.7 μm, the reference spectra only contain the IR spectra of plasmonic structure. Then, the measured spectra of the device with CO_2 were normalized to the reference spectra. Therefore, the spectra in the manuscript only account the IR absorption from CO_2. In order to determine the enhancement provided by the device, an analysis was performed as illustrated in figure 4(d). Since the reference does not have any enhancement, the absorption is purely due to the CO_2 inside the gas cell. According to the Beer–Lambert law, the absorption coefficient α of the CO_2 inside the gas cell without the hybrid plasmonic–MOF device can be calculated using the following equation:

$$I_{out}/I_{in} = \exp(-\alpha \cdot L), \quad (1)$$

where L is the path length of the gas cell. For the gas cell with the hybrid plasmonic–MOF device, besides the CO_2 absorption

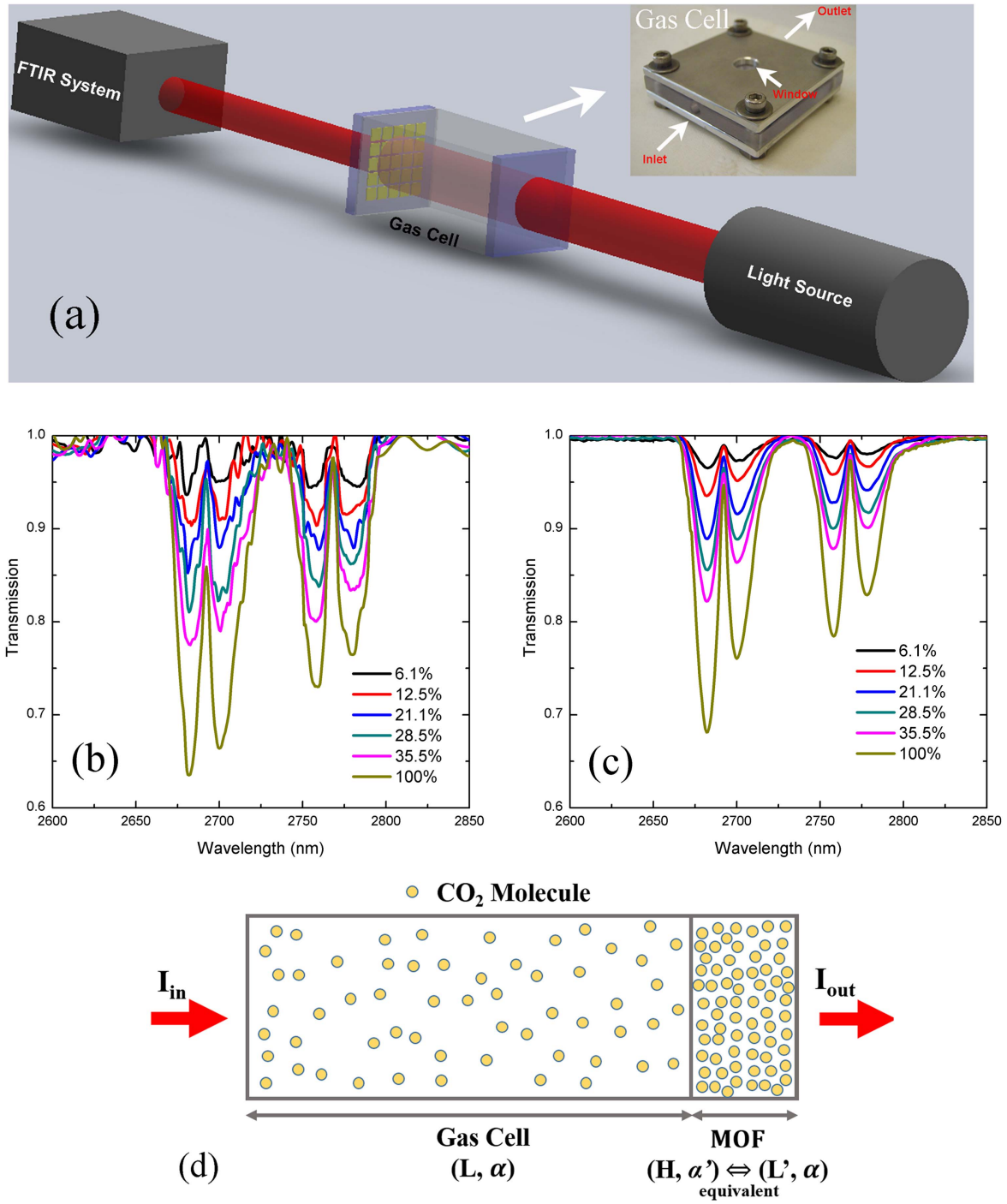

Figure 4. (a) Schematic of the experimental setup for gas sensing. Experimentally obtained transmission spectra of CO_2 for (b) Au-NPA coated with MOF at different CO_2 concentrations and (c) the reference. (d) Illustration of data analysis.

in the gas cell, there is extra IR absorption from CO_2 molecules adsorbed inside the MOF. Therefore, the total IR absorption can be expressed as:

$$I_{out}/I_{in} = \exp(-\alpha \cdot L - \alpha' \cdot H), \quad (2)$$

where α' is the enhanced IR absorption coefficient of the CO_2 adsorbed inside MOF layer, which is larger than α. Since the IR absorption is only exponentially proportional to the product of absorption coefficient and optical path length, equation (2) can be rewritten as equation (3):

$$I_{out}/I_{in} = \exp(-\alpha \cdot L - \alpha \cdot L'). \quad (3)$$

In equation (3), L' is the equivalent optical path length provided by the plasmonic–MOF device, which has a physical length of H. Therefore, the enhancement factor (EF) is defined as $EF = L'/H$. The EF includes both the plasmonic field enhancement effect and also the gas concentrating effect from the MOF film. The calculated EF as a function of CO_2 is shown

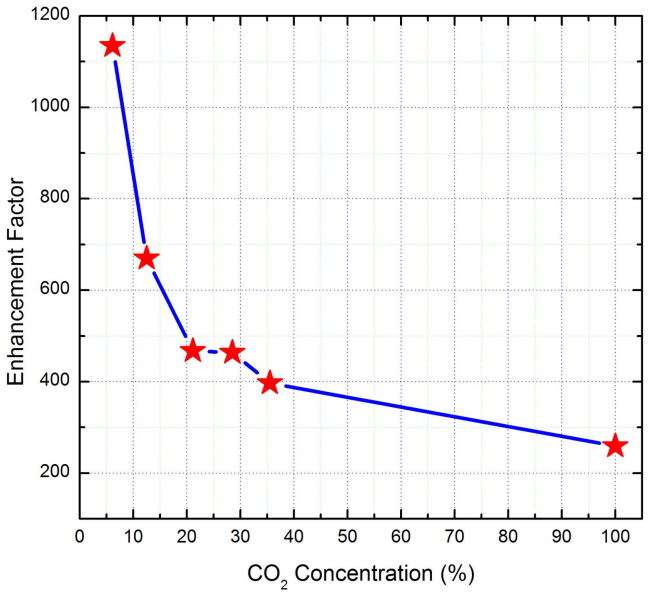

Figure 5. Enhancement factor of Au-NPA coated with MOF as a function of CO_2 concentration.

in figure 5 using the experimental data in figure 4, with the highest EF over 1100. The nonlinear trend is due to the nonlinear absorption behavior of MOF, which is possibly due the different adsorption mechanism at high and low CO_2 concentration as we discussed in [4]. At high concentration, most of the gas molecules are physically adsorbed inside the MOF pores, which are limited by the available space. While at low concentration CO_2, chemical bond adsorption becomes dominant [7, 8], which can provide a large gas concentration factor.

In summary, we present a hybrid plasmonic–MOF device by integrating plasmonic NPA with nano-porous ZIF-8 MOF thin film. Compared with plasmonic NPs-enhanced MOF film, this new type of rationally designed nanophotonic devices provide enhanced optical transmission, higher Q-factors, stronger light–matter interaction, and tunable plasmonic resonances to match the vibrational spectra of the analytes. In this work, the hybrid plasmonic NPA-MOF thin film device was integrated with a gas cell for CO_2 sensing at 2.7 μm wavelength. Based on Beer–Lambert law, the total EF was calculated according to the experimental results. The highest EF obtained is about 1100. This device can be applied for on-chip IR gas sensing, which can potentially reduce the absorption length of conventional gas cells by several orders of magnitude.

This technical effort was sponsored by the National Science Foundation under Grant No. 1449383. Xinyuan Chong and Yujing Zhang were partially supported by the Graduate Student Fellowship from the National Energy Technology Laboratory (NETL).

References

[1] Sneddon G, Greenaway A and Yiu H H P 2014 The potential applications of nanoporous materials for the adsorption, separation, and catalytic conversion of carbon dioxide *Adv. Energy Mater.* **4** 1301873

[2] Li L J, Tang S F, Wang C, Lv X X, Jiang M, Wu H Z and Zhao X B 2014 High gas storage capacities and stepwise adsorption in a UiO type metal-organic framework incorporating Lewis basic bipyridyl sites *Chem. Commun.* **50** 2304–7

[3] Tylianakis E, Klontzas E and Froudakis G E 2009 The effect of structural and energetic parameters of MOFs and COFs towards the improvement of their hydrogen storage properties *Nanotechnology* **20** 204030

[4] Brown C M, Liu Y, Yildirim T, Peterson V K and Kepert C J 2009 Hydrogen adsorption in HKUST-1: a combined inelastic neutron scattering and first-principles study *Nanotechnology* **20** 204025

[5] Li Q and Thonhauser T 2012 A theoretical study of the hydrogen-storage potential of $(H_2)_4CH_4$ in metal organic framework materials and carbon nanotubes *J. Phys.: Condens. Matter* **24** 424204

[6] Levine D J *et al* 2016 Olsalaiine-based metal-organic frameworks as biocompatible platforms for H2 adsorption and drug delivery *J. Am. Chem. Soc.* **138** 10143–50

[7] Chong X, Kim K-J, Li E, Zhang Y, Ohodnicki P R, Chang C-H and Wang A X 2016 Near-infrared absorption gas sensing with metal-organic framework on optical fibers *Sensors Actuators* B **232** 43–51

[8] Chong X Y, Kim K J, Ohodnicki P R, Li E W, Chang C H and Wang A X 2015 Ultrashort near-infrared fiber-optic sensors for carbon dioxide detection *IEEE Sens. J.* **15** 5327–32

[9] Kim K J, Chong X Y, Kreider P B, Ma G H, Ohodnicki P R, Baltrus J P, Wang A X and Chang C H 2015 Plasmonics-enhanced metal-organic framework nanoporous films for highly sensitive near-infrared absorption *J. Mater. Chem.* C **3** 2763–7

[10] Hu Z H, Tao C A, Wang F, Zou X R and Wang J F 2015 Flexible metal-organic framework-based one-dimensional photonic crystals *J. Mater. Chem.* C **3** 211–6

[11] Wu C D and Lin W B 2007 Heterogeneous asymmetric catalysis with homochiral metal-organic frameworks: network-structure-dependent catalytic activity *Angew. Chem., Int. Ed.* **46** 1075–8

[12] Ma L Q, Falkowski J M, Abney C and Lin W B 2010 A series of isoreticular chiral metal-organic frameworks as a tunable platform for asymmetric catalysis *Nat. Chem.* **2** 838–46

[13] Cao H, Zhu S Q, Yang C, Bao R Q, Tong L N, Hou L R, Zhang X G and Yuan C Z 2016 Metal-organic-framework-derived two-dimensional ultrathin mesoporous hetero-ZnFe2O4/ZnO nanosheets with enhanced lithium storage properties for Li-ion batteries *Nanotechnology* **27** 465402

[14] Hyeonseok Y, Alexander W, Wei G, Jinsub C and Engelbert R 2017 Electrodeposition of WO_3 nanoparticles into surface mounted metal-organic framework HKUST-1 thin films *Nanotechnology* **28** 115605

[15] Tilgner D and Kempe R 2017 A plasmonic colloidal photocatalyst composed of a metal-organic framework core and a gold/anatase shell for visible-light-driven wastewater purification from antibiotics and hydrogen evolution *Chemistry* **23** 3184–90

[16] Zhao M T, Deng K, He L C, Liu Y, Li G D, Zhao H J and Tang Z Y 2014 Core–shell palladium nanoparticle@metal-organic frameworks as multifunctional catalysts for cascade reactions *J. Am. Chem. Soc.* **136** 1738–41

[17] Hu P, Morabito J V and Tsung C K 2014 Core–shell catalysts of metal nanoparticle core and metal-organic framework shell *ACS Catalysis* **4** 4409–19

[18] Gao S T, Liu W H, Shang N Z, Feng C, Wu Q H, Wang Z and Wang C 2014 Integration of a plasmonic semiconductor with a metal-organic framework: a case of Ag/AgCl@ZIF-8 with enhanced visible light photocatalytic activity *RSC Adv.* **4** 61736–42

[19] Li Y T, Tang J L, He L C, Liu Y, Liu Y L, Chen C Y and Tang Z Y 2015 Core–shell upconversion nanoparticle@metal-organic framework nanoprobes for luminescent/magnetic dual-mode targeted imaging *Adv. Mater.* **27** 4075–80

[20] Kreno L E, Greeneltch N G, Farha O K, Hupp J T and Van Duyne R P 2014 SERS of molecules that do not adsorb on Ag surfaces: a metal-organic framework-based functionalization strategy *Analyst* **139** 4073–80

[21] He L, Liu Y, Liu J, Xiong Y, Zheng J, Liu Y and Tang Z 2013 Core–shell noble-metal@metal-organic-framework nanoparticles with highly selective sensing property *Angew. Chem., Int, Ed.* **52** 3741–5

[22] Sugikawa K, Nagata S, Furukawa Y, Kokado K and Sada K 2013 Stable and functional gold nanorod composites with a metal-organic framework crystalline shell *Chem. Mater.* **25** 2565–70

[23] Houk R J T, Jacobs B W, El Gabaly F, Chang N N, Talin A A, Graham D D, House S D, Robertson I M and Allendorf M D 2009 Silver cluster formation, dynamics, and chemistry in metal-organic frameworks *Nano Lett.* **9** 3413–8

[24] Hu Y L, Liao J, Wang D M and Li G K 2014 Fabrication of gold nanoparticle-embedded metal-organic framework for highly sensitive surface-enhanced raman scattering detection *Anal. Chem.* **86** 3955–63

[25] Yu T H, Ho C H, Wu C Y, Chien C H, Lin C H and Lee S 2013 Metal-organic frameworks: a novel SERS substrate *J. Raman Spectrosc.* **44** 1506–11

[26] Sugikawa K, Furukawa Y and Sada K 2011 SERS-active metal-organic frameworks embedding gold nanorods *Chem. Mater.* **23** 3132–4

[27] Zhao Y B *et al* 2015 Mesoscopic constructs of ordered and oriented metal-organic frameworks on plasmonic silver nanocrystals *J. Am. Chem. Soc.* **137** 2199–202

[28] Ren F H, Wang X G, Li Z A, Luo J D, Jang S H, Jen A K Y and Wang A X 2014 Enhanced third harmonic generation by organic materials on high-Q plasmonic photonic crystals *Opt. Express* **22** 20292–7

[29] Kreno L E, Hupp J T and Van Duyne R P 2010 Metal-organic framework thin film for enhanced localized surface plasmon resonance gas sensing *Anal. Chem.* **82** 8042–6

[30] Ren F H, Kim K Y, Chong X Y and Wang A X 2015 Effect of finite metallic grating size on Rayleigh anomaly-surface plasmon polariton resonances *Opt. Express* **23** 28868–73

[31] Moharam M G and Gaylord T K 1981 Rigorous coupled-wave analysis of planar-grating diffraction *J. Opt. Soc. Am.* **71** 811–8

[32] Steele J M, Moran C E, Lee A, Aguirre C M and Halas N J 2003 Metallodielectric gratings with subwavelength slots: optical properties *Phys. Rev.* B **68** 205103

[33] Gao H, McMahon J M, Lee M H, Henzie J, Gray S K, Schatz G C and Odom T W 2009 Rayleigh anomaly-surface plasmon polariton resonances in palladium and gold subwavelength hole arrays *Opt. Express* **17** 2334–40

[34] Tian F Y, Mosier A M, Park A, Webster E R, Cerro A M, Shine R S and Benz L 2015 *In situ* measurement of CO2 and H2O adsorption by ZIF-8 films *J. Phys. Chem.* C **119** 15248–53